The glass formation and crystallization studies on iron phosphate–silicate glasses

Justyna Kuczek[1] · Justyna Sułowska[1] · Radosław Lach[1] · Magdalena Szumera[1]

Abstract

The assessment of impact of incorporation of various amount of Fe_2O_3 at the expense of MgO and CaO on the glassy phase formation and thermal stability exhibited in P_2O_5–SiO_2–K_2O–MgO–CaO–Fe_2O_3 system was carried out. The characteristic temperatures for iron phosphate–silicate glasses and glass-crystalline materials were designated from associated DSC curves. Selected samples were subjected to the process of induced crystallization, and products combined with particular exothermic effects were identified. Combination of DSC, XRD and SEM–EDS methods enabled to collect invaluable data concerning the course of crystallization of not only iron phosphate–silicate glasses subjected to the process of induced crystallization, but also glass-crystalline materials obtained directly through melt-quenched technique. The amount of particular crystalline products associated with selected devitrificates was determined via Rietveld technique. Results of the conducted study indicated that Fe_2O_3 addition conduces to the decrease in crystallization temperatures and thermal stability which was reflected in calculated values of ΔT and K_W parameters. Concomitantly, glass with 20 mol% iron (III) oxide addition exhibited significantly improved, distinctive thermal stability among the materials in the analyzed series. The connection of crystalline phases with gradual alterations in polymerization degree of glass matrix was also established. The performed study is a contribution to the knowledge of iron phosphate glasses family and associated glass-crystalline materials.

Keywords Glass-forming ability · Crystallization process · Fe_2O_3 · Iron phosphate–silicate glasses

Introduction

Extensive research conducted on amorphous phosphate solids indicated their interesting fundamental properties. Various phosphate glasses with appropriate chemical composition were considered to be applicable in laser devices [1–4], as highly toxic, radioactive waste storage [5–7] and hermetic seals [5, 8], in electrochemical devices [9], for biomedical usage [10–13], [8]. Nevertheless, their practical use is limited because of poor chemical durability and difficulties in obtaining glassy material resulted from the tendency to crystallization exhibited during processing [8].

It was confirmed that iron (III) oxide addition conduces to the significant improvement of chemical durability. As an example of the utility, the application as nuclear waste host can be mentioned [14, 15]. Moreover, in [15] the increase in counteraction to crystallization in lead metaphosphate glass along with iron ions incorporation was also stated.

Thermal characteristics of phosphate glasses from the simple P_2O_5–Fe_2O_3 system [16] indicate that the crystallization of iron phosphate glasses runs in two stages, and the Fe^{2+}/Fe^{3+} ratio is an important factor which has an influence on this process. The dominant crystalline phases produced by heat treatment are $Fe_3(PO_4)_2$ and $FePO_4$, respectively. During the heat treatment of iron phosphate glasses, crystallization of by-products such as Fe_2O_3, FeO, $Fe_3(PO_4)_2 \cdot xH_2O$ and $FePO_4 \cdot xH_2O$ was concluded. The modification of the composition of this two-component system by addition of

✉ Justyna Kuczek
jkuczek@agh.edu.pl

✉ Magdalena Szumera
mszumera@agh.edu.pl

1 Faculty of Material Science and Ceramics, AGH University of Science and Technology, Al. Mickiewicza 30, 30-059 Cracow, Poland

CaO causes a change in their thermal characteristics. Results of analysis of $xCaO–(40 − x)Fe_2O_3–60P_2O_5$ glasses [17] indicate that with the addition of CaO, thermal stability (ΔT) calculated from the difference between the glass transition and crystallization temperature increases from 79 °C $(x = 0)$ to 96 °C $(x = 40)$. Simultaneously, temperature of crystallization tends to increase to the certain point from 596 °C $(x = 0)$ to 660 °C $(x = 24)$ and then decrease (628 °C for $x = 40$). As it turns out, substitution of CaO in the analyzed system by MgO does not cause significant changes in the thermal characteristics. Glasses from $(40 − x)MgO–xFe_2O_3–60P_2O_5$ system were also analyzed in [18] which exhibited similar tendency. Magnesium ions implementation is associated with the alteration of thermal stability from 61 °C $(x = 40)$ to 239 °C $(x = 0)$ and temperature of the first crystallization effect from 560 °C $(x = 0)$ to 784 °C $(x = 40)$. Additionally, the products of crystallization were also stated as $Mg(PO_3)_2$ $(x = 0)$, $Fe(PO_3)_3$ $(x = 10)$, $Fe_3(P_2O_7)_2$ $(x = 20)$ and $FePO_4$ $(x = 30)$ [18].

The aim of this work is to designate the glass-forming ability exhibited in analyzed system, gather the information about the course of crystallization, identify the associated crystalline products and their connection with structural changes deduced from spectroscopic studies described in [19] and delineate thermal characteristics of glass-crystalline materials with chemical composition not included in glass-forming region.

Experimental

Iron phosphate–silicate glasses and associated glass-crystalline materials from $P_2O_5–SiO_2–K_2O–MgO–CaO–Fe_2O_3$ system were prepared via melt-quenched technique. The molar ratios of P_2O_5/SiO_2 and MgO/CaO were set as 41:6 and 1.5:1. Each material is named with the preservation of information about the molar content of Fe_2O_3 (for example, 2Fe41P corresponds to 2 mol% Fe_2O_3 addition). Batches were prepared through mixing of high-purity ammonium dihydrogen phosphate, silicon dioxide, potassium carbonate, calcium carbonate, magnesium oxide and ferric oxide in ceramic mortar with a pestle in order to obtain desirable homogeneity. The losses concluded from volatility were also taken into account. Batches were melted in a ceramic crucible at 1100 °C in electrical furnace in air atmosphere and quenched by pouring on a steel plate which results in obtaining the materials characterized by similar thermal history.

Chemical composition of four distinctive amorphous solids with 2, 8, 15 and 30 mol% iron (III) oxide addition and the confirmation of their amorphous state can be also found in [19]. The obtained materials are considered compatible with the assumptions. Moreover, amorphous state of additional materials was examined via X-ray diffraction analysis. The results are exemplified in Table 1.

Thermal stability was determined by differential scanning calorimetry (DSC) measurements conducted on Netzsch STA 449 F3 Jupiter 7 operating in the heat flux DSC mode. The temperature and heat calibrations of the instrument were performed using the melting temperatures and melting enthalpies of high-purity materials (Al, Zn, Sn, Au and Ag). Forty-five milligrams of carefully weighed samples was heated in platinum crucibles at 10 °C min^{-1} in air atmosphere up to 1100 °C. The glass transformation temperature T_g was determined as the midpoint of the c_p changes in the glass transformation region. The crystallization temperatures T_{c1} and T_{c2} were ascertain at the maximum deflection point of the exothermal effect. Further

Table 1 Nominal chemical composition of analyzed materials from $P_2O_5–SiO_2–K_2O–MgO–CaO–Fe_2O_3$ system (mol%)

No.	SiO_2	P_2O_5	K_2O	MgO	CaO	Fe_2O_3	Amorphous/crystalline
2Fe41P	6.0	41.0	6.0	27.0	18.0	2.0	A
4Fe41P	6.0	41.0	6.0	25.8	17.2	4.0	A
8Fe41P	6.0	41.0	6.0	23.4	15.6	8.0	A
15Fe41P	6.0	41.0	6.0	19.2	12.8	15.0	A
20Fe41P	6.0	41.0	6.0	16.2	10.8	20.0	A
25Fe41P	6.0	41.0	6.0	13.2	8.8	25.0	A
30Fe41P	6.0	41.0	6.0	10.2	6.8	30.0	A
32Fe41P	6.0	41.0	6.0	9.0	6.0	32.0	A
33Fe41P	6.0	41.0	6.0	8.4	5.6	33.0	A
34Fe41P	6.0	41.0	6.0	7.8	5.2	34.0	C
40Fe41P	6.0	41.0	6.0	4.2	2.8	40.0	C
45Fe41P	6.0	41.0	6.0	1.2	0.8	45.0	C
47Fe41P	6.0	41.0	6.0	–	–	47.0	C

A fully amorphous, *C* glass-crystalline material

data were designated by applying the Netzsch Proteus Thermal Analysis Program (version 5.0.0.).

The fraction containing the particle size of 0.1–0.3 mm was separated for selected glasses and glass-crystalline materials in order to proceed with the isothermal heating for 12 h at the crystallization temperatures designated from the DSC measurements. Crystalline products were identified by XRD method.

Phase composition of the devitrificates obtained from selected samples was designated by X-ray diffraction analysis (X'Pert Pro, Empyrean, Panalytical), and the Rietveld refinement was used to determine quantitative phase content. The internal standard method (Al_2O_3) was used to evaluate the content of the amorphous phase in studied glass-crystalline materials.

The FEI Nova NanoSEM 200 scanning electron microscope was used to perform SEM–EDS observations of the investigated materials. The observations were conducted in high vacuum conditions, with backscatter electron detector (BSED); the accelerated voltage was 18 kV.

Analysis of iron phosphate–silicate glass material and the evaluation of glass formation in studied system

Results of XRD analysis imply the 33 mol% and 0.83 to be the limit values of iron (III) oxide addition and associated Fe/(Fe + Ca + Mg) ratio of the fully amorphous material with the highest amount of incorporated Fe_2O_3 (Fig. 1). The further addition of Fe_2O_3 leads to the formation of glass-crystalline materials.

The SEM–EDS analysis performed on the selected samples with decreased level of amorphousness allowed to detect the regions characterized by different chemical composition (Fig. 2). The thermal characteristic was carried out in the wide range of the chemical composition—not only the fully amorphous samples were analyzed but also the selected one with iron (III) oxide addition exceeded 33 mol% (Fig. 3).

The results of DSC analysis indicate that the analyzed heated-up iron phosphate–silicate glasses, modified with the addition of Fe_2O_3 (from 2 to 47 mol%), undergo the thermodynamic transformation characteristic for glasses, i.e., glass transition, crystallization and melting. The effect of chemical composition on the selected thermal parameters is shown in Fig. 3 and summarized in Table 2.

As can be seen in DSC curves (Fig. 3), glass transition effect is pronounced in samples up to 45 mol% Fe_2O_3 addition and parallelly confirms the presence of glassy phase in glass-crystalline materials containing magnesium and calcium ions, independently from the rate of iron (III) oxide incorporation. Concomitantly, results of the X-ray diffraction analysis carried for 40Fe41P and 45Fe41P corroborate that the gradual Fe_2O_3 addition is combined with the increase in the level of crystallinity. Particularly, the associated amount of amorphous phase is 81.5% (40Fe41P) and 78.4% (45Fe41P). Thus, it is postulated that materials from P_2O_5–SiO_2–K_2O–MgO–CaO–Fe_2O_3 system with previously exemplified correlations between the content of particular oxides, are characterized by significant amorphous phase-forming ability.

The 45Fe41P is the glass-crystalline material in the analyzed series characterized by the highest incorporation of Fe_2O_3 with minor content of magnesium and calcium ions in the structure. Collected X-ray diffraction data were considered to be sufficient for qualitative and quantitative determination of crystalline phases. Therefore, the analysis was carried out without inducing the crystallization process through isothermal heating, which was required for 40Fe41P.

Fig. 1 X-ray diffraction image associated with the verification of amorphous state of selected samples from P_2O_5–SiO_2–K_2O–MgO–CaO–Fe_2O_3 system
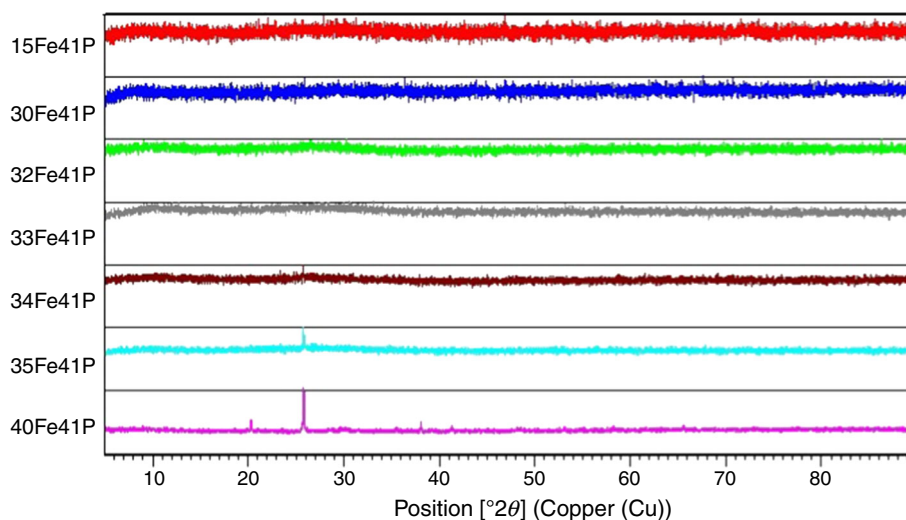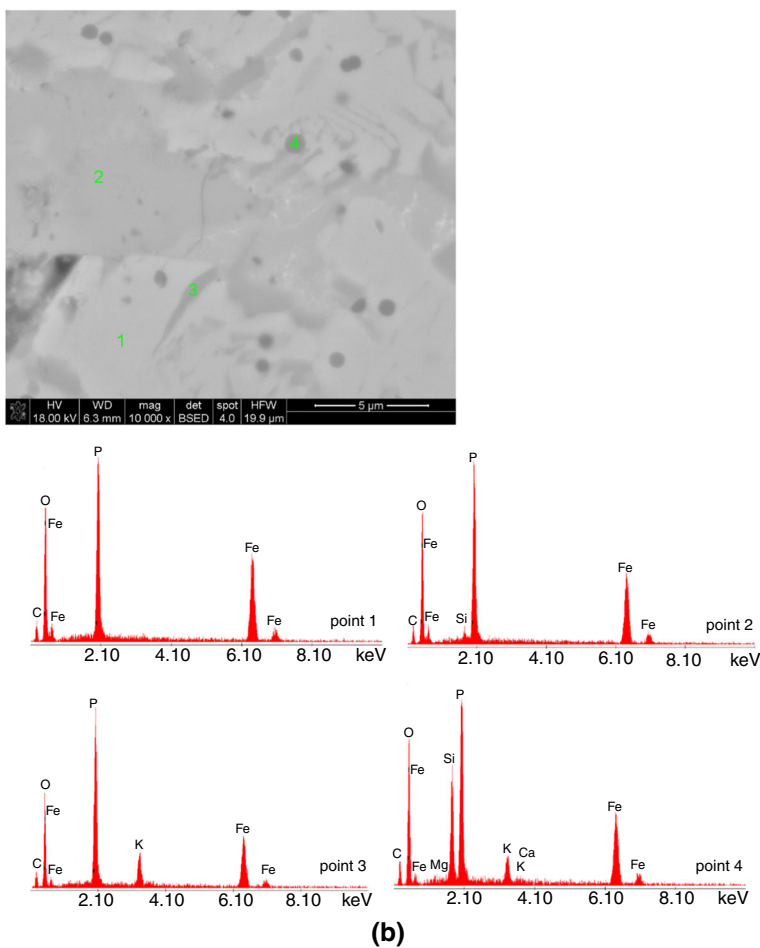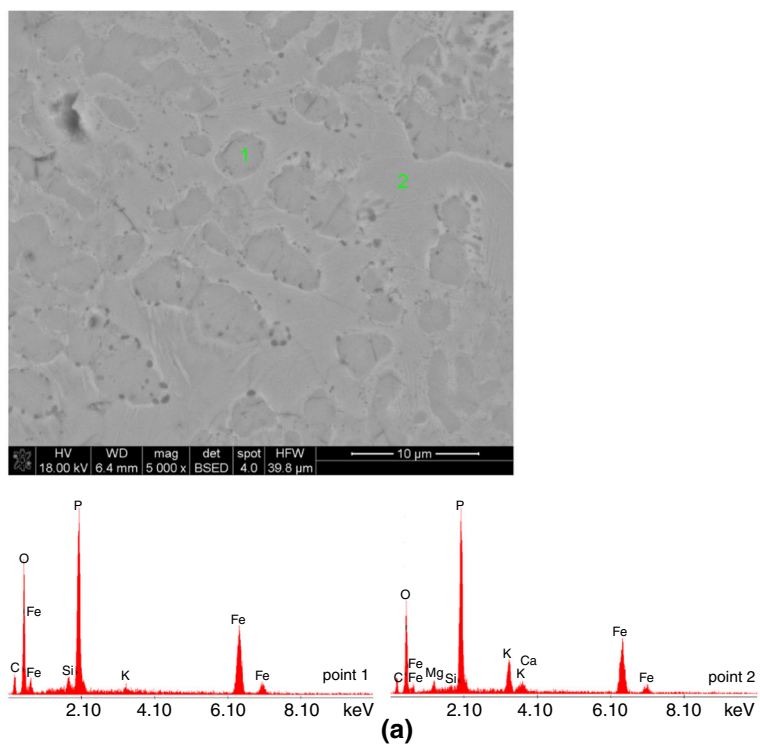
Fig. 2 a SEM–EDS
microphotographs of 40Fe41P
sample. **b** SEM–EDS
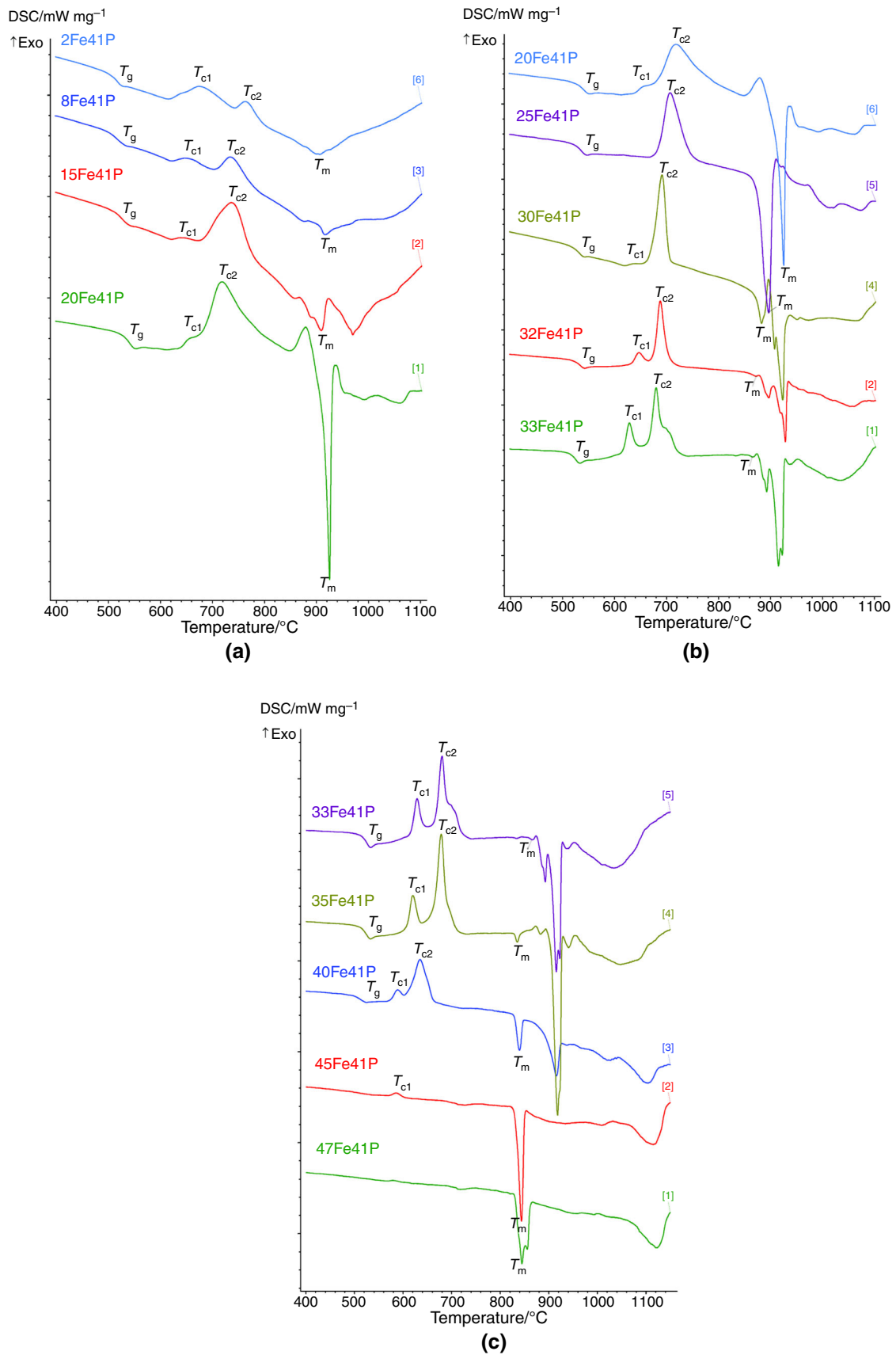microphotographs of 45Fe41P
sample

Fig. 3 DSC curves of analyzed glasses and glass-crystalline materials

Table 2 A summary of characteristic parameters designated from obtained DSC curves, calculated thermal stability parameters and parameters calculated from the chemical composition of the iron phosphate–silicate glasses and glass-crystalline materials

	2Fe41P	4Fe41P	8Fe41P	15Fe41P	20Fe41P	25Fe41P	30Fe41P
O/P/–	3.3	3.4	3.5	3.7	3.8	3.9	4.0
Fe/(Fe + Ca + Mg)/–	0.08	0.16	0.29	0.48	0.60	0.69	0.78
T_g/°C	512	512	514	524	537	532	528
T_{c1}/°C	675	651	646	639	653	707	642
T_{c2}/°C	763	739	735	737	718	–	691
T_m/°C	907	872	916	909	925	897	883
ΔT/°C	163	139	132	115	116	175	114
K_W/–	0.18	0.16	0.14	0.13	0.13	0.20	0.13

	32Fe41P	33Fe41P	35Fe41P	40Fe41P	45Fe41P	47Fe41P
O/P/–	4.1	4.1	4.1	4.3	4.4	4.4
Fe/(Fe + Ca + Mg)/–	0.81	0.83	0.85	0.92	0.98	1.0
T_g/°C	529	522	521	513	–	–
T_{c1}/°C	647	629	619	589	586	581
T_{c2}/°C	688	680	679	635	–	–
T_m/°C	874	866	835	839	844	844
ΔT/°C	118	107	98	76		
K_W/–	0.14	0.12	0.12	0.09		

40Fe41P and 45Fe41P glass-crystalline materials exhibit the presence of three distinctive phases, such as $FePO_4$, $FeKP_2O_7$ and $Fe_7(PO_4)_6$. The Rietveld analysis performed for 40Fe41P revealed that the content of each products is influenced by the heating temperature (Table 3). Concomitantly, the corresponding amount of particular phases designated for 45Fe41P is varied. Particularly, the fraction of $Fe_7(PO_4)_6$ is increased to 42.5%, content of $FePO_4$ is relatively less influenced (38.3%), and $FeKP_2O_7$ is reduced to 19.2%.

In the microphotographs of the samples obtained by SEM–EDS (Fig. 2), regions rich in phosphorus and iron, and also with phosphorus, iron and potassium, were featured. It supports the acquired data correlated with crystallization of $FeKP_2O_7$, $Fe_7(PO_4)_6$ and $FePO_4$ phases and confirms that mentioned elements tend to be incorporated into crystalline products to a considerable degree compared to magnesium, silicon and calcium.

Additionally, the relatively small area enriched with silicon is found. The minor concentrations of magnesium and calcium are also detected. Considering the results of qualitative analysis of crystalline products carried out by X-ray diffraction method, it can be postulated that silicon, magnesium and calcium are more likely originated from the amorphous phase, which is present in the sample in a significant amount (81.5% for 40Fe41P and 78.4% for 45Fe41P). It can be explained through the evaluation of ionicity of the chemical bonds ("i_G") and the binding electron location parameter ("L") which are measures of the elasticity of the vitreous bond and the rigidity of chemical bonds, respectively [20].

Analysis of ionicity values of chemical bonds for P–O ($i_{G\ P-O} = 0.314$; $L = 2.640$) and Si–O ($i_{G\ Si-O} = 0.428$; $L = 2.410$) [20] clearly indicates that lower value of elasticity of bonds will result in greater tendency to the destruction of the glass structure. Therefore, the silicate network is stronger and requires higher energy to be destroyed which contributes to the impediment of the crystallization of silicates [21]. Thus, only the crystallization of phosphates is observed.

Analysis of iron phosphate–silicate glasses and glass-crystalline materials after the induced crystallization process

The multistage crystallization of glasses from P_2O_5–SiO_2–K_2O–MgO–CaO–Fe_2O_3 system exhibits exothermic, partially overlapped effects (T_{c1} and T_{c2}) exposed in associated DSC curves (Fig. 3a–c). The course of the process in analyzed multicomponent system is influenced by a wide range of factors such as physicochemical factors, chemical affinity, the assumptions about the rate of magnesium and calcium ions substitution (Fe/(Fe + Ca + Mg)) and even the fractions of di- and trivalent iron ions. In order to explain the progressive alterations occurring with gradual Fe_2O_3 incorporation at the expense of MgO and CaO, the corresponding crystalline products were assigned via XRD.

Table 3 The kind of crystallizing phases identified in the analyzed devitrificates

	4Fe41P	8Fe41P	15Fe41P	25Fe41P	30Fe41P	32Fe41P	35Fe41P	40Fe41P
T_{c1}								
Phase 1	$KMg(PO_3)_3$	$FeKP_2O_7$	$FeKP_2O_7$	–	Un	$FeKP_2O_7$	$FeKP_2O_7$	$FeKP_2O_7$
Ref. code	IGOD 01-074-2002	ICSD 98-020-2814	ICSD 98-008-6309	–	–	ICSD 98-020-2814	ICSD 98-020-2814	ICSD 98-020-2814
Fraction/%	–	–	–	–	–	46.7	31.1	25.1
Free enthalpy/ kJ mol^{-1}	− 5820.86	− 4009.50	− 4009.50	–	–	− 4009.50	− 4009.50	− 4009.50
Phase 2	$CaMgP_2O_7$	$CaMgP_2O_7$	–	–	Un	$FePO_4$	$FePO_4$	$FePO_4$
Ref. code	IGOD 00-024-0135	IGOD 00-024-0135	–	–	–	ICSD 98-041-2737	ICSD 98-041-2742	ICSD 98-041-2742
Fraction/%	–	–	–	–	–	53.3	47.6	40.9
Free enthalpy/ kJ mol^{-1}	− 4622.33	− 4622.33	–	–	–	− 2122.18	− 2122.18	− 2122.18
Phase 3	–	–	–	–	–	–	$Fe_7(PO_4)_6$	$Fe_7(PO_4)_6$
Ref. code	–	–	–	–	–	–	ICSD 98-002-0765	ICSD 98-002-0765
Fraction/%	–	–	–	–	–	–	21.3	34.0
Free enthalpy/ kJ mol^{-1}	–	–	–	–	–	–	− 13,080.5	− 13,080.5
T_{c2}								
Phase 1	$Mg_2(PO_3)_4$	$FeKP_2O_7$	$FeKP_2O_7$	$FeKP_2O_7$	$FeKP_2O_7$	$FeKP_2O_7$	$FeKP_2O_7$	$FeKP_2O_7$
Ref. code	ICSD 98-000-4280	ICSD 98-020-2814	ICSD 98-008-6309	ICSD 98-009-6309	IGOD 01-084-1798	ICSD 98-020-2814	ICSD 98-020-2814	ICSD 98-020-2814
Fraction/%					51.8	53.4	33.6	25.0
Free enthalpy/ kJ mol^{-1}	− 8023.05	− 4101.97	− 4101.97	− 4101.97	− 4101.97	− 4101.97	− 4101.97	− 4009.50
Phase 2	$CaMgP_2O_7$	$CaMgP_2O_7$	$CaMgP_2O_7$	$Fe_3(PO_4)_2$	$FePO_4$	$FePO_4$	$FePO_4$	$FePO_4$
Ref. code	IGOD 00-024-0135	IGOD 00-024-0135	IGOD 00-024-0135	98-028-1704	IGOD 01-070-1793	ICSD 98-041-2737	ICSD 98-041-2742	ICSD 98-041-2742
Fraction/%					48.2	46.6	35.2	36.8
Free enthalpy/ kJ mol^{-1}	− 4709.98	− 4709.98	− 4709.98	− 4333.25	− 2169.40	− 2169.40	− 2169.40	− 2122.18
Phase 3	–	–	–	–	–	–	$Fe_7(PO_4)_6$	$Fe_7(PO_4)_6$
Ref. code	–	–	–	–	–	–	ICSD 98-002-0765	ICSD 98-002-0765
Fraction/%	–	–	–	–	–	–	31.2	38.2
Free enthalpy/ kJ mol^{-1}	–	–	–	–	–	–	− 13,376.2	− 13,080.5

Un unidentified

Results of performed spectroscopic analysis conducted on P_2O_5–SiO_2–K_2O–MgO–CaO–Fe_2O_3 glasses have provided interesting data about the structure of analyzed materials [19]. The main conclusion is that Fe_2O_3 addition leads to the progressive depolymerization of the phosphorus subnetwork and increase in the content of ferric ions both tetrahedrally and octahedrally coordinated at the expense of ferrous ions. The rate of depolymerization degree is revealed by O/P ratio which also suggests the kind of prevailing phosphate units [22]. The alterations in chemical composition are reflected through individual parameter, similarly as in [23]. Due to the fact that iron (III) oxide is incorporated at the expense of MgO and CaO, it was decided to present the nominal changes via Fe/(Fe + Ca + Mg) ratio which decreases with the increase in content of calcium and magnesium ions. The limited value calculated from nominal chemical composition of glass containing the comparable amount of iron oxide and magnesium and calcium oxide (17.6 mol% and 11.8 mol%, respectively) is set as 0.54.

Results of Raman study [19] indicate that phosphorus subnetwork of glasses with lower iron (III) oxide addition not exceeded by 4 mol% is built from metaphosphate units to a considerable degree. A distinctive spectra of 4Fe41P and 8Fe41P implicate that 8Fe41P is structurally more influenced through progressive discontinuity of the network and crucial role of pyrophosphate units. The structure undergoes a major transformation with further iron (III) oxide addition. Similarly as Raman spectra, DSC curves are gradually altered and it is combined with variation of products of the multistage crystallization (Fig. 3, Table 3).

As can be seen in Fig. 3a, multistage crystallization process exhibited by glasses with Fe/(Fe + Ca + Mg) ratio not exceeded 0.29 (marked as 2Fe41P and 8Fe41P) proceeds in wider temperature range, especially compared to glasses with at least 30 mol% Fe_2O_3 addition (Fig. 3b, c).

Relatively small effects in wide temperature range presented in curves of glasses with lower iron (III) oxide addition, such as 2Fe41P considered as highly polymerized, and 8Fe41P are due to crystallization of phases enriched with links with greater ionicity ($i_{G\ K-O} = 0.823$, $i_{G\ Ca-O} = 0.707$, $i_{G\ Mg-O} = 0.670$) such as $KMg(PO_3)_3$ and $CaMgP_2O_7$ (T_{c1}), $Mg_2(PO_3)_4$ and $CaMgP_2O_7$ (T_{c2}) in 4Fe41P (Fig. 4a) and $CaMgP_2O_7$ (T_{c1} and T_{c2}) in 8Fe41P in which $FeK(P_2O_7)$ was also found (Table 3).

The results of assignment presented in Table 3 also indicate that more polymerized phosphates were detected only in samples with a slight addition of Fe_2O_3 not exceeded 4 mol% ($KMg(PO_3)_3$ and $Mg_2P_4O_{12}$). It supports the conclusions of spectroscopic analysis. It is also presumable that due to the calculated values of ΔG, $KMg(PO_3)_3$ and $Mg_2(PO_3)_4$ are privileged in comparison

with $CaMgP_2O_7$ (Table 3). Furthermore, bonds with more ionic character have superior elasticity and require more energy to be broken which is also reflected in the relatively wider range of crystallization temperatures exhibited in curve and also implies that the structure of glasses with lower iron (III) oxide addition is thermally strengthen.

Commencing from 15Fe41P sample, the second exothermic peak is gaining on distinctiveness compared to the first effect. Simultaneously, the general tendency of crystallization temperatures to decrease and intensification of melting effects with the increase in (Fe/(Fe + Ca + Mg)) parameter is also presented.

It can be stated that the increase in distinctiveness of the second crystallization peak (Fig. 3) is probably combined with crystallization of iron-rich phosphate phases (Table 2) in which besides another possible joints, such as strongly ionic K–O linkage in $FeKP_2O_7$, more covalent Fe^{3+}–O bonds are marked. This is also the result of progressive decrease in magnesium and calcium ions content in the analyzed series of materials. The character of Fe^{3+}–O links indicates the increased rigidity and it requires lower energy for its destruction. It also explains the general tendency to decrease the crystallization temperatures along with the increase in Fe/(Fe + Ca + Mg) parameter.

Additionally, the first crystallization effect is influenced. It may be deducted from Fig. 3a, b that it decreases and its assigned maximum temperature is altered which leads to the reduction in visible separateness and simultaneously results in emergence of the single peak at 707 °C (25Fe41P curve). However, it is again revealed in 30Fe41P curve, and from that point, it becomes to be more distinct.

Products assigned to the first visible crystallization effect also reflect the strong influence of chemical composition variations revealed by Fe/(Fe + Ca + Mg) ratio. As it was mentioned before, obtained phases associated with samples with iron (III) oxide addition not exceeded 4 mol% are enriched with magnesium, potassium and calcium ions and possess a significant polymerization degree. Induced crystallization of 15Fe41P and 20Fe41P glasses leads to the formation of one phase named as iron potassium diphosphate (Table 3). The pronounced alteration is observed in 25Fe41P curve. 25Fe41P glass crystallization seems to be simplified and is displayed by single, less broaden peak in 707 °C associated with $FeK(P_2O_7)$ and $Fe_3(PO_4)_2$. The specific character of this curve needs to be explained by the key impact of $Fe_3(PO_4)_2$, which apparently influences the crystallization of $FeKP_2O_7$ through increasing the temperature of the process. Thus, appearance of $Fe_3(PO_4)_2$ is directly connected to the exhibition of single presumably overlapped effect in the mentioned DSC curve.

The stoichiometry of the $Fe_3(PO_4)_2$ phase may be linked to the ferrous ions. It was concluded in [19] that the
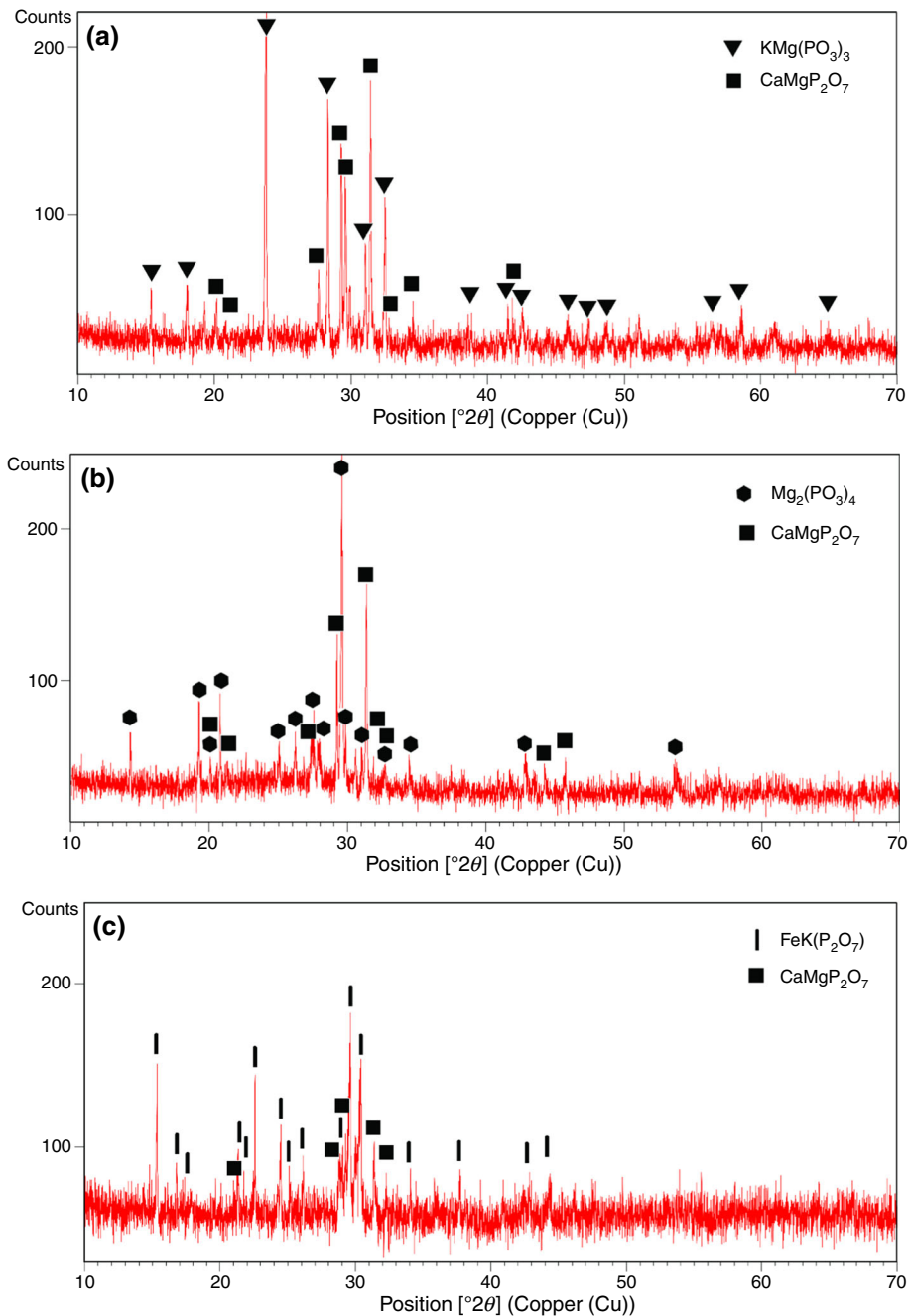
Fig. 4 XRD pattern and the assignment of crystalline phases conducted for **a** 4Fe41P (T_{c1}), **b** 4Fe41P (T_{c2}), **c** 15Fe41P (T_{c2}), **d** 25Fe41P (T_{c2}) and **e** 30Fe41P (T_{c2}) glasses subjected to the process of induced crystallization

increase in iron (III) oxide incorporation in analyzed system generally causes the increase in ferric ions at the expense of ferrous ions. Nevertheless, the presence of Fe^{2+} ions was confirmed for 30Fe41P via Mössbauer spectroscopy. The appearance of $Fe_3(PO_4)_2$ needs to be explained by predominance of Fe_2O_3 (25 mol%) over MgO (13.2 mol%) and CaO (8.8 mol%) and the insufficient amount of magnesium and calcium ions for their incorporation into crystalline products.

The reappearance of the first effect (T_{c1}) in 30Fe41P curve and the alterations such as decrease in its assigned temperatures and distinctiveness visible in further curves up to 33Fe41P, are implied from the change of the type of crystallization products, particularly the vanishing of $Fe_3(PO_4)_2$ and appearance of $FePO_4$. It could not have been reflected in experimental results collected from 30Fe41P glass due to the proximity of the effects; however, it was succeeded for 32Fe41P sample (Table 3).
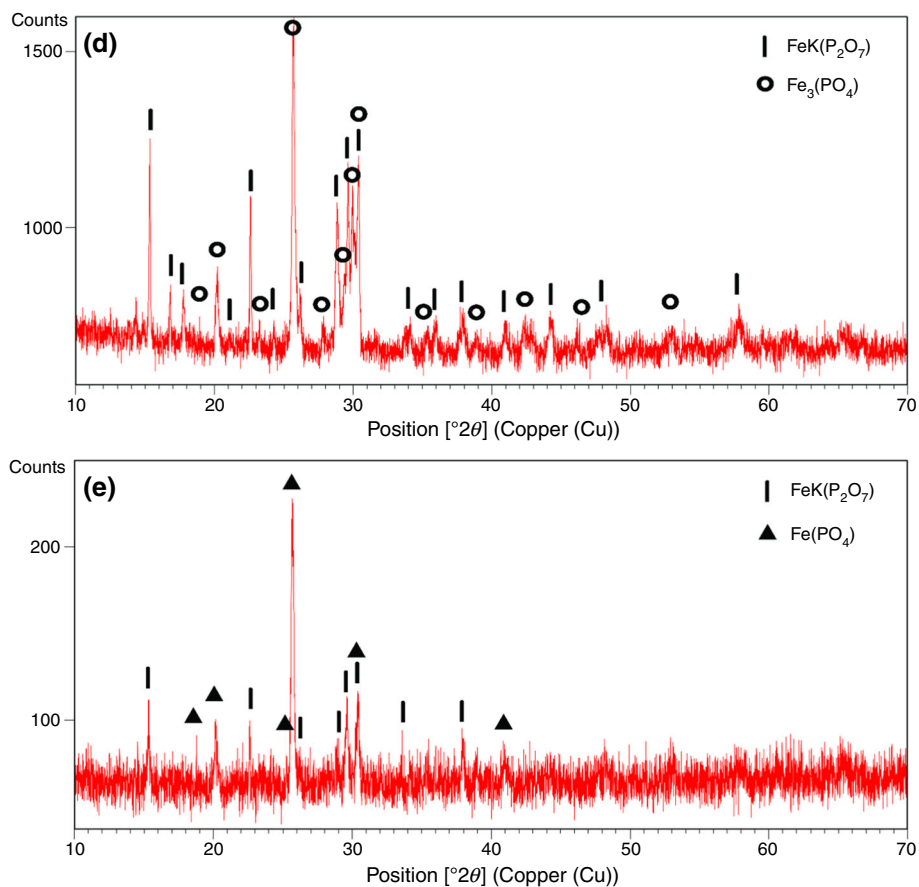
Fig. 4 continued

For further considerations, the Rietveld analysis was carried out for 30Fe41P, 32Fe41P, 35Fe41P and 40Fe41P samples subjected to the process of induced crystallization. Obtained results are presented in Fig. 5 and Table 3. Crystallization effects exhibited in curves of 30Fe41P and 32Fe41P glasses are associated with the presence of $FeKP_2O_7$ and $FePO_4$. Further iron (III) oxide addition leads to the obtaining of glass-crystalline materials characterized also by the presence of $Fe_7(PO_4)_6$. The content of phases designated through Rietveld analysis varies depending on the Fe/(Fe + Ca + Mg) ratio and the temperature of combined exothermic effect.

The content of $FePO_4$ is increased compared to $FeKP_2O_7$ in 30Fe41P and 32Fe41P samples in the second crystallization effect (T_{c2}, Fig. 3). The opposite results were obtained for the first crystallization effect (T_{c1}). It may be presumed that crystallization of $FeKP_2O_7$ should be more associated with the second crystallization effect and in T_{c1} $FePO_4$ is more privileged.

The occurrence of $Fe_7(PO_4)_6$ is attributed to the general decrease in amount of $FePO_4$ and particularly $FeKP_2O_7$ in T_{c2} (Fig. 5). Increasing content of $Fe_7(PO_4)_6$ at the expense of $FeKP_2O_7$ indicates the change in the type of
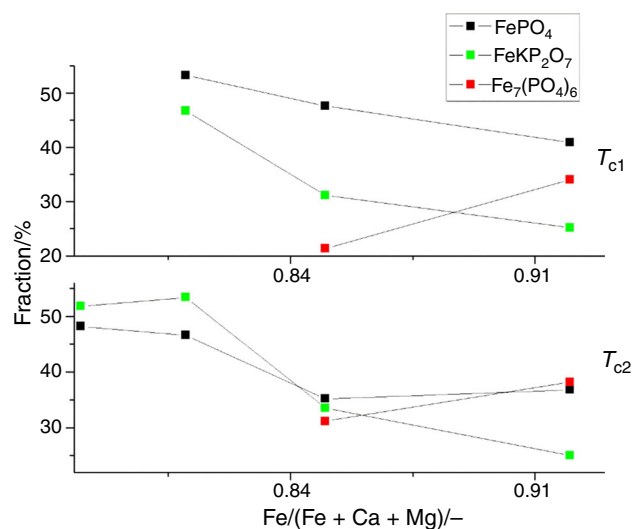

Fig. 5 Graphical presentation of results of Rietveld analysis for 30Fe41P (Fe/(Fe + Ca + Mg) = 0.78), 32Fe41P (Fe/(Fe + Ca + Mg) = 0.81), 35Fe41P (Fe/(Fe + Ca + Mg) = 0.85), 40Fe41P (Fe/(Fe + Ca + Mg) = 0.92)

polymerization degree. It implies that ferric ions may exhibit the cross-linking character and also leads to the progressive ordering of the structure.

Thermal stability of iron phosphate–silicate glasses

In order to express thermal stability of iron phosphate–silicate glasses, characteristic temperatures associated with thermal effects were designated through DSC curves. ΔT [°C] and K_W [–] parameters [23] were calculated accordingly to Eqs. 1 and 2. Results are included in Table 2 and in Fig. 6.

$$\Delta T = T_{c1} - T_g \tag{1}$$

$$K_W = (T_{c1} - T_g)/T_m \tag{2}$$

It can be concluded that with gradual iron (III) oxide incorporation, ΔT and K_W are influenced and the general tendency to decrease is revealed. Significantly polymerized 2Fe41P glass with Fe/(Fe + Ca + Mg) ratio as 0.08 possesses the improved thermal stability and reduced susceptibility to crystallization ($\Delta T = 163$ °C and $K_W = 0.18$) compared to 30Fe41P glass ($\Delta T = 107$ °C and $K_W = 0.12$, Fe/(Fe + Ca + Mg) = 0.78).
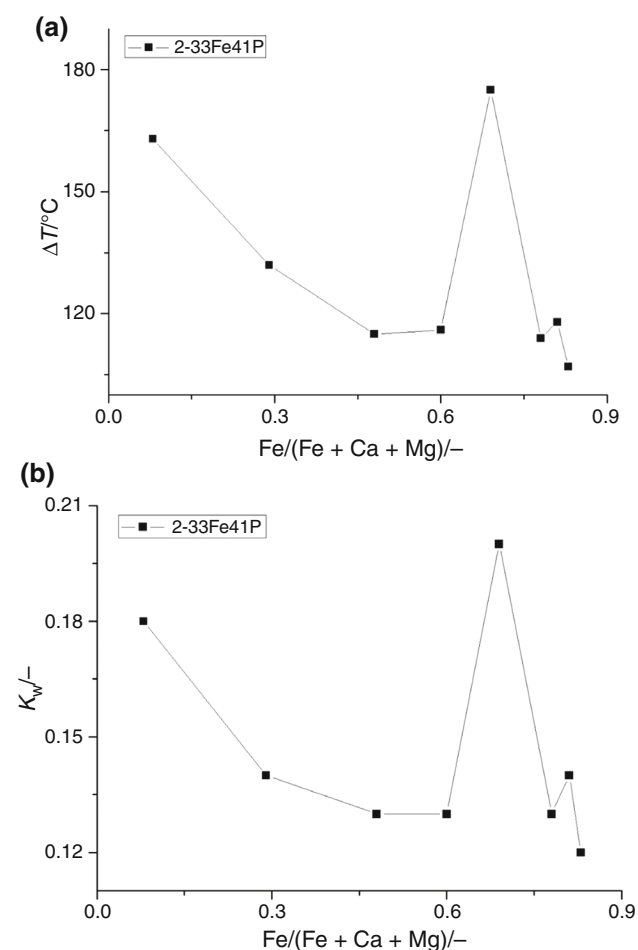
(a)

(b)

Fig. 6 Graphical representation of thermal stability parameters calculated from Eqs. 1 (**a**) and 2 (**b**)

It needs to be noted that 25Fe41P glass with matched 0.69 as value of Fe/(Fe + Ca + Mg) ratio does not follow this trend, and it reveals surprisingly superior thermal stability in comparison with glasses with lower Fe_2O_3 addition, manifested by higher values of ΔT and K_W parameters equal to 175 °C and 0.20. It is directly connected to reflected alterations in DSC curves and as it was ascribed, the effect of crystallization of $Fe_3(PO_4)_2$ phase is crucial.

The general tendency to decrease thermal stability parameters was maintained with extension of consideration to glass-crystalline materials for which the designation of glass transition temperatures was possible (35Fe41P and 40Fe41P).

Conclusions

Glass formation in P_2O_5–SiO_2–K_2O–MgO–CaO–Fe_2O_3 system was evaluated. 33 mol% addition was estimated as the limit value of Fe_2O_3 which enables to obtain a fully amorphous material. Further iron ions implementation conduces to the increase in the level of crystallinity. Nevertheless, the designated content of amorphous phase in 40Fe41P (81.5%) and 45Fe41P (78.4%) glass-crystalline materials is still tremendous. Nevertheless, the glass-forming region is considerably wide.

Results of DSC, XRD and SEM–EDS analysis indicated that silicon ions are presumably more associated with amorphous phase detected in all analyzed samples. More energy is required for breaking of Si–O bonds due to greater elasticity, manifested itself through the value of iG parameter, compared to P–O bond which simultaneously clarifies this phenomenon.

Calcium magnesium diphosphate, iron potassium diphosphate and iron (III) phosphate are considered as frequently appearing phases. $CaMgP_2O_7$ was detected after induced crystallization in analyzed samples characterized by Fe/(Fe + Ca + Mg) parameter not exceeded 0.60 value (20Fe41P). Thus, products enriched with calcium and magnesium ions are not observed in samples prepared from glasses containing less than 16.2 mol% MgO and 10.8 mol% CaO and more than 20 mol% Fe_2O_3. Parallelly, $FeKP_2O_7$ is identified in every sample with Fe/(Fe + Ca + Mg) ratio higher than 0.16. It is associated with the appearance of phosphates which are less polymerized compared to the $KMg(PO_3)_3$ and $Mg_2(PO_3)_4$ phases observed in 4Fe41P sample. The inherence of $FePO_4$ was confirmed for glasses and glass-crystalline materials containing at least 30 mol% Fe_2O_3. It is presumable that magnesium-rich and calcium-rich phases reveal the minor tendency to crystallization compared to products enriched

with iron ions, and it was concluded based on the alterations presented in DSC curves.

Iron (III) oxide addition leads to the decrease in the thermal stability of the glasses. However, 25Fe41P glass is characterized by significantly improved thermal stability parameters which implies it greater resistance to crystallization process. It is correlated with a crystallization of specific phase ($Fe_3(PO_4)_2$).

In glass-crystalline materials, the presence of $FePO_4$, $FeKP_2O_7$ and $Fe_7(PO_4)_6$ phases was also stated due to proceeding with induced crystallization in samples containing 35 and 40 mol% Fe_2O_3. It is consistent with results obtained for 45Fe41P. The amount of $Fe_7(PO_4)_6$ is increasing at the expense of $FePO_4$ and $FeKP_2O_7$. It is presumably combined with proceeding of the ordering in the structure. It may also imply the cross-linking ability manifested by iron ions.

References

1. Yin Qianwen, Kang Shuai, Wang Xue, Li Shunguang, He Dongbing, Lili Hu. Effect of PbO on the spectral and thermo-optical properties of Nd^{3+}-doped phosphate laser glass. Opt Mater. 2017;66:23–8.

2. Pisarski WA, Żur L, Goryczka T, Sołtys M, Pisarska J. Structure and spectroscopy of rare earth–Doped lead phosphate glasses. J Alloys Compd. 2014;587:90–8.

3. Podniesiński D, Nakielska M, Kozłowska A, Stępień R, Pysz D. Erbium, ytterbium and chromium doped phosphate glass laser. Electron Mater. 2015;43(1):4–10.

4. Hu L, He D, Chen H, Wang X, Meng T, Wen L, Hu J, Xu Y, Li S, Chen Y, Chen W, Chen S, Tang J, Wang B. Research and development of neodymium phosphate laser glass for high power laser application. Opt Mater. 2017;63:213–20.

5. Stoch P, Stoch A, Ciecińska M, Krakowiak I, Sitarz M. Structure of phosphate and iron-phosphate glasses by DFT calculations and FTIR/Raman spectroscopy. J Non-Cryst Solids. 2016;450:48–60.

6. Ojovan MI, Lee WE. Immobilisation of radioactive waste in glass. In: Ojovan MI, Lee WE, editors. An introduction to nuclear waste immobilisation. 2nd ed. Amsterdam: Elsevier; 2014. p. 245–82.

7. Wacławska I, Szumera M. Fosforanowe materiały ceramiczne do immobilizacji kadmu w środowisku glebowym. Ceram Mater. 2011;63(2):407–12.

8. Sales BC. Phosphate glasses. Mater Res Soc. 1987;12:32–4.

9. Brow RK. Review: the structure of simple phosphate glasses. J Non-Cryst Solids. 2000;263&264:1–28.

10. Abou Neel EA, Ahmed I, Pratten J, Nazhat SN, Knowles JC. Characterisation of antibacterial copper releasing degradable phosphate glass fibres. Biomaterials. 2005;26:2247–54.

11. Ahmed I, Shaharuddin SS, Sharmin N, Furniss D, Rudd C. Core/clad phosphate glass fibres containing iron and/or titanium. Biomed Glasses. 2015;1:20–30.

12. Mishra A, Rocherullé J, Massera J. Ag-doped phosphate bioactive glasses: thermal, structural and in vitro dissolution properties. Biomed. Glasses. 2016;2:38–48.

13. Yang JH, Park H-S, Cho Y-Z. Silver phosphate glasses for immobilization of radioactive iodine. Ann Nuclear Energy. 2017;110:208–14.

14. Stoch P, Szczerba W, Bodnar W, Ciecińska M, Stoch A, Burkel E. Structural properties of iron-phosphate glasses: spectroscopic studies and ab initio simulations. Phys Chem Chem Phys. 2014;16(37):19917–27.

15. Sales BC, Ramsey RS, Bates JB, Boatner IA. Investigation of the structural properties of lead-iron phosphate glasses using liquid chromatography and raman scattering spectroscopy. J Non-Cryst Solids. 1986;87:137–58.

16. Doupovec J, Sitek J, Kakos J. Crystallization of iron phosphate glasses. J Therm Anal. 1981;22:213–9.

17. Li HJ, Liang XF, Yu HJ, Yang DQ, Yang SY. Studies of structure of calcium–iron phosphate glasses by infrared, Raman and UV–Vis spectroscopies. Indian J Phys. 2016;90(6):693–8.

18. Mošner P, Račický A, Koudelka L. Thermal properties and crystallization of $MgO–FeOx–P_2O_5$ glasses. J Thermal Anal Calorimet. 2018;132(2):843–50.

19. Kuczek J, Jelen P, Stoch P, Błachowski A, Wacławska I, Szumera M. Raman and Mossbauer studies of iron phosphate–silicate glasses. J Mol Struct. 2018;1170:82–9.

20. Görlich E. The effective nuclear charges and the electronegativity. Kraków: Polish Academy of Art and Science; 1997.

21. Stoch L. Structure and crystallization of multicomponent glasses. Proc Int Congr Glass. 2001;1:62–73.

22. Liebau F. The influence of cation properties on the conformation of silicate and phosphate anions. In: Navrotsky A, O'Keeffe M, editors. Structure and bonding in crystals. Cambridge: Academic Press; 1981. p. 198.

23. Ma L, Brow RK, Ghussn L, Schlesinger ME. Thermal stability of $Na_2O–FeO–Fe_2O_3–P_2O_5$ glasses. J Non-Cryst Solids. 2015;409:131–8.

Publisher's Note Springer Nature remains neutral with regard to jurisdictional claims in published maps and institutional affiliations.